Journal of Materials Chemistry C

ROYAL SOCIETY OF CHEMISTRY

PAPER

View Article Online
View Journal | View Issue

Cite this: J. Mater. Chem. C, 2021, 9, 3177

Reducing the reverse leakage current of AlGaN/GaN heterostructures *via* low-fluence neutron irradiation

Rong Wang, *[ab] Jianxing Xu,[a] Shiyong Zhang,[a] Ying Zhang,[a] Penghui Zheng,[a] Zhe Cheng,[cd] Lian Zhang,[cd] Feng-Xiang Chen,[e] Xiaodong Tong,[a] Yun Zhang[cd] and Wei Tan*[a]

Reduction of the reverse leakage current is critical to AlGaN/GaN heterostructures in high power and high frequency applications. Taking AlGaN/GaN Schottky barrier diodes (SBDs) as an example, we demonstrate both theoretically and experimentally that low-fluence neutron irradiation can be a promising way to reduce the reverse leakage current while maintaining other electronic properties almost unchanged. A clear physical picture is given to elucidate the mechanism, which includes three main scenarios: (i) in pre-irradiated AlGaN/GaN heterostructures grown by metal organic chemical vapor deposition (MOCVD) on sapphire substrates, the configuration of threading dislocations (DLs) is the mixture of pure DLs and DLs decorated by group-III vacancies (V_{III}-DLs); (ii) neutron scattered group-III interstitials are mobile and prone to passivate V_{III}-DLs, changing the configuration of DLs to monomorphic pure DLs; (iii) after the saturation of the passivation, neutron scattered group-III interstitials begin to escape from the system. The physical analysis is consistent with the trends in the experimental data. Our work provides a new post-processing treatment for reducing the reverse leakage current of AlGaN/GaN heterostructures grown by MOCVD on sapphire substrates.

Received 1st December 2020,
Accepted 25th January 2021

DOI: 10.1039/d0tc05652a

rsc.li/materials-c

Introduction

AlGaN/GaN heterostructures possess a series of advantages such as wide bandgaps, high breakdown fields, high saturation electron drift velocities, high radiation-tolerance and strong polarization.[1–4] Owing to the optimization of material growth and device fabrication, especially defect control throughout the processing, AlGaN/GaN heterostructures have achieved great success in high-frequency and high-power applications involving harsh environments.[2–4] However, in many applications, the reverse leakage current significantly deteriorates the performance of AlGaN/GaN heterostructures. Taking AlGaN/GaN high electron mobility transistors (HEMTs) as example, in high-power-oriented AlGaN/GaN HEMTs, the reverse leakage current increases the gate leakage current, narrows the voltage range for the safe operation of gates and increases the power consumption of AlGaN/GaN HEMTs.[5] For high-frequency-oriented AlGaN/GaN HEMTs, the reverse leakage current results in an off-state leakage, which reduces the device operation efficiency and degrades the off-state reliability of AlGaN/GaN HEMTs.[6] Therefore, reducing the reverse leakage current is critical to AlGaN/GaN heterostructures in higher power and higher frequency applications.

It was found that threading dislocations play a dominate role in leakage paths for reversely biased AlGaN/GaN devices.[7,8] Hence, the most common approach to reduce the reverse leakage current of AlGaN/GaN heterostructures is to reduce the concentration of threading dislocations by optimizing the substrate and growth conditions.[9,10] It was found that the following approaches could reduce the reverse leakage current of AlGaN/GaN heterostructures: (i) surface passivation and optimization of the AlGaN barrier;[11–13] (ii) optimization of the Schottky metal which improves the Schottky barrier height;[14] and (iii) adoption of lattice-matched barrier alloys such as InAlN, ScAlN and ScGaN to decrease the concentration of threading dislocations and enhance the piezoelectric effect.[15–17] However, each of the above-mentioned approaches involves either the change of the epitaxy wafers or the change of the process flow, which significantly increases the production cost and processing complexity.

[a] Microsystem and Terahertz Research Center, Institute of Electronic Engineering, China Academy of Engineering Physics, Chengdu 610200, China. E-mail: rong_wang@zju.edu.cn, weitan@csrc.ac.cn
[b] Hangzhou Global Scientific and Technological Innovation Center, Zhejiang University, Hangzhou, 311200, China
[c] Institute of Semiconductors, Chinese Academy of Sciences, Beijing 100083, China
[d] University of Chinese Academy of Sciences, Beijing 100049, China
[e] Department of physics, School of Science, Wuhan University of Technology, Wuhan 430070, China

In this work, we propose a new type of post-processing treatment by using the low-fluence neutron irradiation to reduce the reverse leakage current in AlGaN/GaN heterostructures grown by metal organic chemical vapor deposition (MOCVD) on sapphire substrates, while maintaining the high concentration and mobility of the two-dimensional electron-gas (2DEG) almost unchanged. We take AlGaN/GaN Schottky barrier diodes (SBDs) as an example to investigate the physical mechanism for the interaction of low-fluence neutrons and AlGaN/GaN heterostructures. For reversely biased AlGaN/GaN SBDs, the dominant emission mechanism changes from the two-stage Frenkel–Poole (FP) emission to the monomorphic single FP emission after low-fluence neutron irradiation. Microscopically, the physical picture illustrates that the incident neutrons cause the scattering of group-III atoms in the AlGaN barrier, which is prior to passivating the threading dislocations decorated by group-III vacancies (V_{III}-DLs), and thus change the configuration of DLs from the mixture of pure DLs and V_{III}-DLs to monomorphic pure DLs. Our work opens a new pathway to reduce the reverse leakage current of AlGaN/GaN heterostructures grown by MOCVD on sapphire substrates *via* low-fluence neutron irradiation without increasing the processing complexity of AlGaN/GaN devices.

Experimental methods

AlGaN/GaN heterostructures investigated in this work consist of a 21 nm undoped $Al_{0.26}Ga_{0.74}N$ barrier layer and a 2 μm undoped GaN buffer layer on the (0001)-oriented sapphire substrate, which were grown by MOCVD. AlGaN/GaN SBDs were used to investigate the effect of low-fluence neutron irradiation on the electronic properties of AlGaN/GaN heterostructures. The device mesa of AlGaN/GaN SBDs was acquired by Cl_2/BCl_3 plasma dry etching in an ICP-RIE system. Ti/Al/Ti/Au ohmic contacts were deposited and thermally annealed at 870 °C for 45 seconds. The Schottky contact was obtained by Ni/Au e-beam evaporation and lift-off.

Neutron irradiation of AlGaN/GaN SBDs was carried out at the Chinese Fast Burst Reactor-II (CFBR-II) of the Institute of Nuclear Physics and Chemistry, China Academy of Engineering Physics, which provides a controlled 1 meV equivalent fast neutron radiation. AlGaN/GaN SBDs were irradiated with a fluence of 1×10^{14} neutrons cm^{-2} at room temperature, at a fluence rate of 2×10^{9} neutrons/(cm^2 s). Before and after the neutron irradiation, *I–V* measurements were performed on an Agilent B1500 semiconductor parameter analyzer in the temperature range of 298–453 K to analyze the change of the electronic properties of AlGaN/GaN SBDs.

Results and discussion

Effect of neutron irradiation on the electronic properties of AlGaN/GaN SBDs

Fig. 1 shows the current of AlGaN/GaN SBDs before and after the low-fluence neutron irradiation at room temperature. It is clear that the neutron irradiation significantly reduces the reverse current of AlGaN/GaN SBDs by two orders of magnitude while exerting a negligible effect on the forward current.

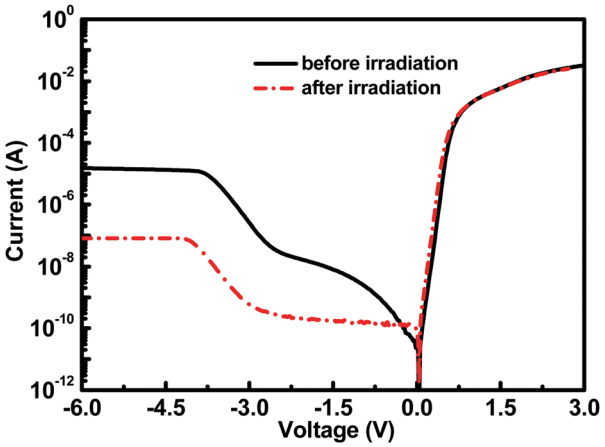

Fig. 1 Current of AlGaN/GaN SBDs before and after neutron irradiation.

In order to investigate the origin of reduced current of the reversely biased AlGaN/GaN SBDs, we carry out temperature dependent *I–V* measurements on reversely biased AlGaN/GaN SBDs before and after low-fluence neutron irradiation. It is widely accepted that the current of reversely biased AlGaN/GaN Schottky diodes is dominated by the Frenkel–Poole (FP) emission. The FP emission is characterized by the thermal emission of electrons from the Schottky metal to the continuum of electronic states in the AlGaN barrier.[18] For AlGaN/GaN heterostructures, the lattice-mismatch and thermal mismatch induce high density of threading dislocations in the AlGaN barrier.[1] The defect states of threading dislocations act as electron-transfer channels in the FP emission.[19] Electrons can be excited by either the temperature or the electronic field. Therefore, the FP current exhibits both temperature and voltage dependence.[20,21] Fig. 2a shows the current of pre-irradiated AlGaN/GaN SBDs as a function of the bias voltage at temperatures ranging from 298 K to 453 K. There are two distinct regions (the first FP and second FP as shown in Fig. 2a) showing two distinct temperature and voltage dependence curves of the current, indicating that there exist two distinct FP emission states for reversely biased AlGaN/GaN SBDs. This is consistent with previous research studies, according to which the two FP emission states correlate with electron-transfer *via* V_{III}-DLs and pure DLs in the AlGaN barrier.[22]

Next, we adopt the FP emission model to estimate the barrier of electron transfer *via* the two kinds of DLs in AlGaN. The FP current is calculated using[23,24]

$$I_{FP} = CE_b A \exp\left[-\frac{q\left(\phi_t - \sqrt{qE_b/\pi\varepsilon_0\varepsilon_s}\right)}{k_B T}\right] \quad (1)$$

where E_b is the electric field, ϕ_t is the barrier height of electron emission from the Schottky metal to the DL state, k_B is the Boltzmann constant, ε_0 and ε_s are the permittivity of free space and the relative dielectric permittivity at high frequency,

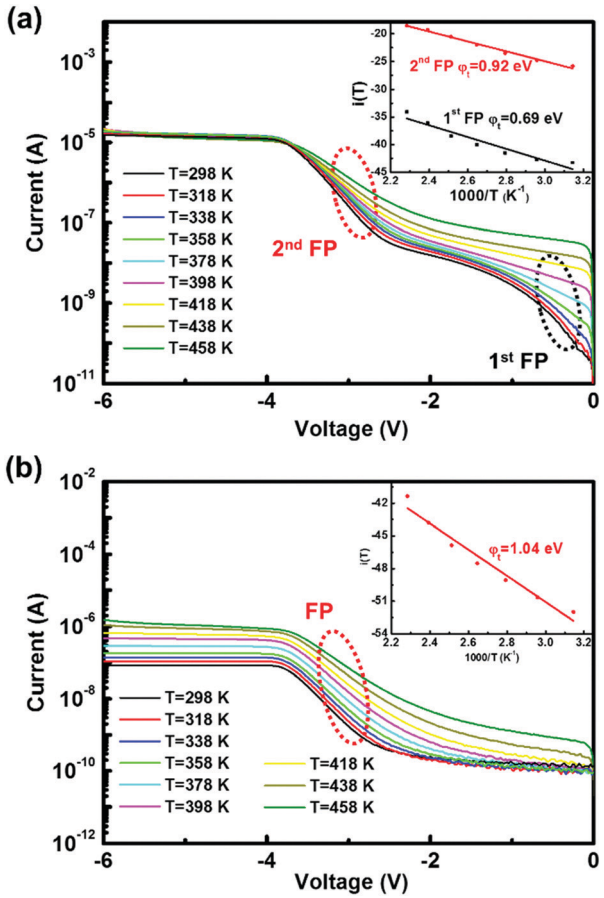

Fig. 2 Temperature-dependent current of AlGaN/GaN SBDs as a function of voltage (a) before and (b) after low-fluence neutron irradiation. The insets show the plots of $i(T)$ *vs.* $1000/T$ before and after low-fluence neutron irradiation.

respectively. Taking logarithms of eqn (1), we have

$$\log\left(\frac{I_{FP}}{E_b}\right) = \log C + \log A + \frac{q}{k_B T}\sqrt{\frac{qE_b}{\pi\varepsilon_0\varepsilon_s}} - \frac{q\phi_t}{k_B T} \equiv s(T)\sqrt{E_b} + i(T) \quad (2)$$

With the slope of $i(T)$ *vs.* $1/T$, we find that the barrier heights for electron transfer *via* V_{III}-DLs and pure DLs are 0.69 eV and 0.92 eV, respectively.

The temperature dependent *I–V* measurements of neutron-irradiated AlGaN/GaN SBDs under the reverse voltage are shown in Fig. 2b. Interestingly, the region of FP emission *via* V_{III}-DLs disappears and the barrier height for electron transfer *via* pure DLs increases to 1.04 eV. This indicates that the state of V_{III}-DLs disappears while the state of DLs shifts to a higher energy upon low-fluence neutron irradiation.

Effect of neutron irradiation on the properties of 2DEG of AlGaN/GaN heterostructures

The properties of 2DEG are another aspect to assess the performance of AlGaN/GaN heterostructures. In order to evaluate the effect of low-fluence neutron irradiation on the properties of 2DEG of AlGaN/GaN heterostructures, transmission line model (TLM) patterns were fabricated on the same wafer of AlGaN/GaN SBDs.[25] The channel lengths of TLM patterns are 5, 10, 15, 30, 60 and 120 μm. *I–V* measurements of TLM structures indicate that the sheet resistance of the 2DEG channel increases slightly from 301 Ω/□ to 319 Ω/□ after the low-fluence neutron irradiation. The sheet resistance is calculated using[25]

$$R_{sh} = \frac{1}{qn_s\mu} \quad (3)$$

where q is the electronic charge, n_s is the 2DEG concentration and μ is the 2DEG mobility. It was found that the low-fluence neutron irradiation only causes scattering and atomic displacement in the AlGaN barrier, so the carrier scattering and thus 2DEG mobility is not affected by the irradiation.[26,27] With the 2DEG mobility of ~1100 $cm^2/V\,s$,[28] the 2DEG concentration of AlGaN/GaN heterostructures decreases from 1.9×10^{13} cm^{-2} to 1.8×10^{13} cm^{-2}. This slight decrease of the 2DEG concentration exerts almost negligible effect on most applications of AlGaN/GaN heterostructures.

Low-fluence neutron irradiation induced evolution of dislocations in the AlGaN barrier

Next, we discuss the microscopic origin of the change of electronic properties of low-fluence neutron irradiated AlGaN/GaN SBDs. We start from the configuration of threading DLs in pre-irradiated AlGaN/GaN heterostructures, discuss the properties of neutron scattered defects, reveal the interactions between neutron scattered defects and threading DLs, and finally clarify the mechanism for the effect of low-fluence neutron irradiation on the electronic properties of AlGaN/GaN heterostructures.

Configuration of threading DLs in pre-irradiated AlGaN/GaN heterostructures

During the epitaxy of the AlGaN/GaN heterostructures, the density of threading DLs is as high as 10^7–10^{11} cm^{-2} due to thermal and lattice mismatch between the heterostructure and its substrates.[29] For pre-irradiated AlGaN/GaN SBDs under the reverse voltage, electrons first transfer along the low-energy states of V_{III}-DLs (corresponding to the first FP emission stage). When the electrons transferring along V_{III}-DLs become saturated, electrons begin to transfer *via* the higher energy states of pure DLs (corresponding to second FP emission stage) as the reverse voltage increases. This is referred to as the two-stage FP emission in reversely biased AlGaN/GaN SBDs before the neutron irradiation, which has been well studied in our previous work.[22] Therefore, the configuration of threading DLs is the mixture of V_{III}-DLs and pure DLs for pre-irradiated AlGaN/GaN heterostructures.[22]

Properties of neutron scattered defects

It is widely accepted that the neutron irradiation induces displacement damage and causes device-degradation of GaN-based devices.[30,31] Because the threshold energy for the atomic displacement of group-III atoms is much smaller than that of N atoms,[3] the low-fluence neutron irradiation causes the scattering

of group-III atoms from their lattice sites to interstitial sites (III_i), leaving excess V_{III} located at their original lattice sites.

In the following, we calculate the diffusion properties of III_i and V_{III} by first-principles calculations. Due to the larger size of Ga compared to that of Al, the diffusion barriers of Ga_i and V_{Ga} are larger than those of Al_i and V_{Al}, respectively. Therefore, we simplify the diffusion properties of III_i and V_{III} in AlGaN alloy to those of Ga_i and V_{Ga} in GaN. According to first-principles defect calculations, Ga_i^{3+} and V_{Ga}^{3-} dominate the charge state of Ga_i and V_{Ga} in n-type GaN.[32] Therefore, we calculate the diffusion properties of V_{Ga}^{3-} and Ga_i^{3+} in wurtzite GaN to evaluate the diffusion properties of neutron scattered defects.

First-principles calculations were carried out within the density functional theory (DFT) framework, as implemented in the Vienna *ab initio* simulation package (VASP).[33,34] The core electrons are treated within the projector augmented wave (PAW) pseudopotentials.[35] The exchange and correlation interaction between electrons are described by the generalized gradient approximation (GGA) formulated by Perdew, Burke, and Ernzerhof (PBE).[36] The plane-wave cutoff for the wavefunction expansion was set to 450 eV. The local minimum of Ga_i and V_{Ga} is obtained by full relaxation of all atoms in the 96-atom supercell until the Hellman–Feynman forces become less than 0.01 eV $Å^{-1}$. The Monkhorst–Pack scheme with a Γ-centered $2 \times 2 \times 2$ special k-point mesh is adopted to sample the reciprocal space of the supercell.[37] The climbing image nudged elastic band (CI-NEB) method was adopted to obtain the minimum diffusion paths and diffusion barrier energies between the initial and final states of Ga_i.[38]

For defects in wurtzite structures, the diffusion path can be either parallel or perpendicular to the [0001] direction (Fig. 3a and d). As shown in Fig. 3b and c, the diffusion barrier of V_{Ga}^{3-} perpendicular to the [0001] direction is about 0.5 eV lower than that parallel to the direction. For the diffusion of V_{Ga}^{3-} parallel and perpendicular to the [0001] direction can be regarded as the diffusion of its out-of-plane and in-plane nearest Ga atoms to the vacancy site, respectively. The equivalence of in-plane Ga atoms causes the lower diffusion barrier of V_{Ga}^{3-} perpendicular to the [0001] direction.

The diffusion of Ga_i only relates to the steric effect, without the bond-breaking in GaN. Therefore, the diffusion barrier of Ga_i^{3+} is lower than that of V_{Ga}^{3-}. Ga_i are stabilized at the channel-centered site and locate closer to the lower plane of Ga atoms. This makes Ga_i equidistant from its six nearest N atoms, minimizing the overlap for the electron cloud of Ga_i and the N atoms. Due to the minimization of the overlap of the electron cloud with the N atoms, the diffusion barrier of Ga_i perpendicular to the [0001] direction is as low as 0.9 eV.

Interaction between neutron scattered defects and threading DLs

As a further step, we evaluate whether Ga_i^{3+} are mobile at room temperature once generated by the scattering of neutrons. During the application and measurement of neutron-irradiated AlGaN/GaN Schottky diodes, the diffusion barrier of Ga_i^{3+} is lowered by the applied electronic field using[39]

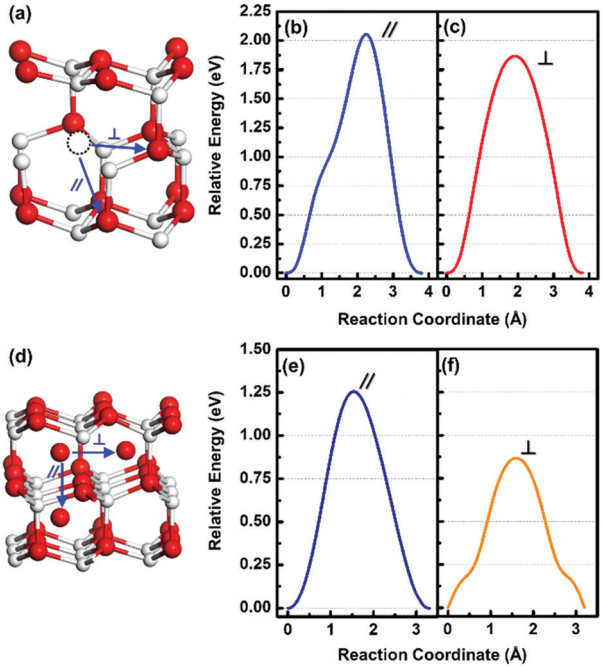

Fig. 3 Atomic structures showing diffusion paths and calculated diffusion barriers of V_{Ga}^{3-} (top panel) and Ga_i^{3+} (bottom panel) in wurtzite GaN.

$$\Delta E_d = E_b q l \quad (4)$$

where E_b is the electronic field along the diffusion direction, $q = 3$ is the charge state of Ga_i^{3+} and l is the diffusion length, which is $\sim$3 Å. With eqn (4), the diffusion barrier for Ga_i^{3+} is lowered by $\sim$0.2 eV.

According to the harmonic transition state theory (HTST), the rate of diffusion is calculated using[39,40]

$$\Gamma^{HTST} = \frac{\prod_i^{3N} \nu_i^{min}}{\prod_i^{3N-1} \nu_i^{saddle}} e^{-\frac{E_b}{k_B T}} = \Gamma_0 e^{-\frac{E_b}{k_B T}} \quad (5)$$

where E_b is the diffusion barrier, ν_i^{min} and ν_i^{saddle} are the $3N$ normal mode frequency at the minimum-energy site and $3N-1$ nonimaginary normal mode frequencies at the saddle point, respectively, k_B is the Boltzmann constant, and Γ_0 is the attempting frequency, which is estimated to be 10^{13} Hz for the interstitials in GaN. Assuming the jumping rate of 1 Hz for Ga_i^{3+} in GaN, the activation temperature for the diffusion of Ga_i^{3+} is estimated to be 271 K. Therefore, Ga_i^{3+} are highly mobile as long as they are scattered by neutrons.

We then illustrate the physical picture for the interaction between neutron scattered defects and threading DLs. As shown in Fig. 4a, the scattering of neutrons mainly take place near the surface of the AlGaN barrier. The neutron scattered III_i are highly mobile. When III_i locate near V_{III}, first-principles calculations indicate that they would recombine together with energy gain. Therefore, the neutron scattered III_i would firstly passivate V_{III}-DLs, thus converting the configuration of threading DLs in AlGaN barrier to pure DLs (process ① as shown in Fig. 4b). When the passivation of V_{III}-DLs becomes saturated, III_i begin to escape from the heterostructure, and leave excess V_{III} in the

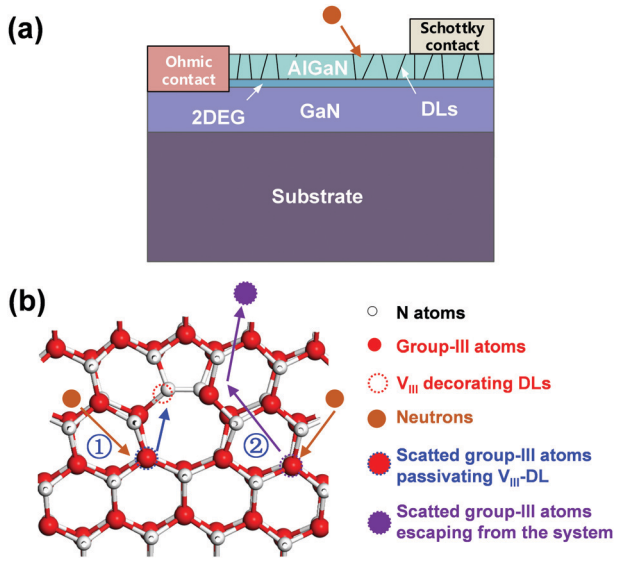

Fig. 4 Schematic diagram showing (a) interaction between the incident neutron and AlGaN/GaN SBDs, (b) interaction between the incident neutron and the AlGaN barrier containing threading DLs.

perfect region of the AlGaN barrier (process ② as shown in Fig. 4b).

Mechanism for the effect of low-fluence neutron irradiation on the electronic properties of AlGaN/GaN heterostructures

Finally, we illustrate the physical mechanism for the effect of low-fluence neutron irradiation on the electronic properties of AlGaN/GaN heterostructures. For pre-irradiated AlGaN/GaN heterostructures, the configuration of DLs is the mixture of pure DLs and V_{III}-DLs, which gives rise to the two-stage FP emission (Fig. 5a). During the neutron irradiation, process ① as shown in Fig. 4b converts the configuration of DLs to monomorphic pure DLs, which causes the disappearance of the first FP emission state of the low-fluence neutron irradiated AlGaN/GaN SBDs. The subsequent process ② as shown in Fig. 4b leaves V_{III} in the perfect region of the AlGaN barrier. V_{III} behave as acceptors in AlGaN,[41] these negatively charged defects rise above the conduction band minimum (CBM) of the AlGaN barrier, and thus increase the energy barrier for electron transfer from the metal Fermi level to the defect states of pure DLs in the AlGaN barrier Fig. 5b. This explains the increase of the ϕ_t for the second FP emission for low-fluence neutron-irradiated AlGaN/GaN SBDs. The upward shift of the CBM of AlGaN also raises the conduction band edge of the GaN channel, thus slightly decreasing the 2DEG concentration for low-fluence neutron-irradiated AlGaN/GaN heterostructures.

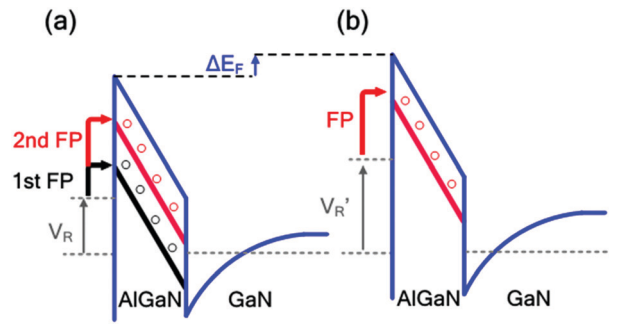

Fig. 5 Schematic band diagram of (a) pre-irradiated and (b) low-fluence neutron-irradiated AlGaN/GaN heterostructures. The black and red lines represent defect levels of V_{III}-DLs and pure DLs, respectively. ΔE_F shows the upward shift of the conduction band of the AlGaN barrier.

It should be noted that the physical mechanism is appropriate for low-fluence neutron irradiated AlGaN/GaN heterostructures grown by MOCVD on the sapphire substrate. The configuration of defects in pre-irradiated AlGaN/GaN heterostructures may be different when the substrate and growth method change.[42,43] The evolution of defects in AlGaN/GaN heterostructures irradiated by neutrons also depends on the energy and fluence of neutrons.[43,44] Therefore, the low-fluence neutron irradiation induced reduction of reverse leakage current needs to be checked for AlGaN/GaN heterostructures grown using other growth methods or other substrates.

Conclusions

In conclusion, we have shown that low-fluence neutron irradiation is promising for reducing the reverse leakage current and maintaining the other electronic properties of AlGaN/GaN devices. The FP emission of reversely biased AlGaN/GaN Schottky diodes changes from two-stage FP emission to monomorphic single FP emission after the low-fluence neutron irradiation. Microscopically, we have revealed that the incident neutrons cause the scattering of group-III atoms in the AlGaN barrier. The scattered group-III atoms firstly passivate the V_{III}-decorated threading DLs, change the configuration of DLs from the mixture of pure DLs and V_{III}-decorated DLs to monomorphic pure DLs. Our work opens a new pathway for reducing the reverse leakage current of AlGaN/GaN heterostructures grown by MOCVD on sapphire substrates *via* low-fluence neutron irradiation without increasing the processing complexity of AlGaN/GaN devices.

Author contributions

R. W. and W. T. conceived the original idea, wrote the first draft and revised the manuscript. R. W. participated in neutron irradiation experiments, carried out electronic measurements and performed first-principles calculations. J. X. and S. Z. fabricated the AlGaN/GaN Schottky barrier diodes, Y. Z. and P. Z. participated in neutron irradiation experiments. Z. C. and L. Z. participated in device-fabrication. F. C. discussed first-principles results. X. T. participated in electronic measurements, data-analysis and results–discussion. Y. Z. provided valuable advice on device-fabrication. All authors have approved the final version of the manuscript.

Conflicts of interest

There are no conflicts to declare.

Acknowledgements

This work was supported by the Science Challenge Program (Grant No. TZ2018003). The National Supercomputer Center in Tianjin is acknowledged for computational support.

Notes and references

1 W. G. Bi, H. H. Kuo, P. Ku and B. Shen, *Handbook of GaN semiconductor materials and devices*, CRC Press, Boca Raton, FL, USA, 2017.
2 R. Quay, *Gallium nitride electronics*, Springer Science & Business Media, Freiburg, Germany, 2008.
3 A. Y. Polyakov, S. J. Pearton, P. Frenzer, F. Ren, L. Liu and J. Kim, *J. Mater. Chem. C*, 2013, **1**, 877.
4 A. Ionascut-Nedelcescu, C. Carlone, A. Houdayer, H. J. Von Bardeleben, J. L. Cantin and S. Raymond, *IEEE Trans. Nucl. Sci.*, 2002, **49**, 2733.
5 N. Xu, R. Hao, F. Chen, X. Zhang, H. Zhang, P. Zhang, X. Ding, L. Song, G. Yu, K. Cheng, Y. Cai and B. Zhang, *Appl. Phys. Lett.*, 2018, **113**, 152104.
6 M. Mi, X. Ma, L. Yang, B. Hou, J. Zhu, Y. He, M. Zhang, S. Wu and Y. Hao, *Appl. Phys. Lett.*, 2017, **111**, 173502.
7 B. Kim, D. Moon, K. Joo, S. Oh, Y. K. Lee, Y. Park, Y. Nanishi and E. Yoon, *Appl. Phys. Lett.*, 2014, **104**, 102101.
8 J. W. P. Hsu, M. J. Manfra, R. J. Molnar, B. Heying and J. S. Speck, *Appl. Phys. Lett.*, 2002, **81**, 79.
9 J. W. P. Hsu, M. J. Manfra, S. N. G. Chu, C. H. Chen, L. N. Pfeiffer and R. J. Molnar, *Appl. Phys. Lett.*, 2001, **78**, 3980.
10 S. E. Bennett, *Mater. Sci. Technol.*, 2013, **26**, 1017.
11 S. Zhang, K. Wei, X.-H. Ma, B. Hou, G.-G. Liu, Y.-C. Zhang, X.-H. Wang, Y.-K. Zheng, S. Huang, Y.-K. Li, T.-M. Lei and X.-Y. Liu, *Appl. Phys. Lett.*, 2019, **114**, 013503.
12 Z. H. Liu, G. I. Ng, H. Zhou, S. Arulkumaran and Y. K. T. Maung, *Appl. Phys. Lett.*, 2011, **98**, 113506.
13 Z. Yuhao, S. Min, W. Hiu-Yung, L. Yuxuan, P. Srivastava, C. Hatem, M. Azize, D. Piedra, Y. Lili, T. Sumitomo, N. A. de Braga, R. V. Mickevicius and T. Palacios, *IEEE Trans. Electron Devices*, 2015, **62**, 2155.
14 J.-H. Shin, J. Park, S. Jang, T. Jang and K. Sang Kim, *Appl. Phys. Lett.*, 2013, **102**, 243505.
15 J. Ren, D. Yan, G. Yang, F. Wang, S. Xiao and X. Gu, *J. Appl. Phys.*, 2015, **117**, 154503.
16 M. A. Moram and S. Zhang, *J. Mater. Chem. A*, 2014, **2**, 6042.
17 S. M. Knoll, S. K. Rhode, S. Zhang, T. B. Joyce and M. A. Moram, *Appl. Phys. Lett.*, 2014, **104**, 101906.
18 E. J. Miller, D. M. Schaadt, E. T. Yu, X. L. Sun, L. J. Brillson, P. Waltereit and J. S. S. Peck, *J. Appl. Phys.*, 2003, **94**, 7611.
19 H. Zhang, E. J. Miller and E. T. Yu, *J. Appl. Phys.*, 2006, **99**, 023703.
20 E. Arslan, S. Bütün and E. Ozbay, *Appl. Phys. Lett.*, 2009, **94**, 142106.
21 W. Chikhaoui, J. M. Bluet, M. A. Poisson, N. Sarazin, C. Dua and C. Bru-Chevallier, *Appl. Phys. Lett.*, 2010, **96**, 072107.
22 R. Wang, X. Tong, J. Xu, C. Dong, Z. Cheng, L. Zhang, S. Zhang, P. Zheng, F.-X. Chen, Y. Zhang and W. Tan, *Phys. Rev. Appl.*, 2020, **14**, 024039.
23 L. Chen, N. Jin, D. Yan, Y. Cao, L. Zhao, H. Liang, B. Liu, E. X. Zhang, X. Gu, R. D. Schrimpf, D. M. Fleetwood and H. Lu, *IEEE Trans. Electron Devices*, 2020, **67**, 841.
24 S. Turuvekere, N. Karumuri, A. A. Rahman, A. Bhattacharya, A. DasGupta and N. DasGupta, *IEEE Trans. Electron Devices*, 2013, **60**, 3157.
25 M. Asif Khan, M. S. Shur and Q. Chen, *Appl. Phys. Lett.*, 1996, **68**, 3022.
26 A. Y. Polyakov, N. B. Smirnov, A. V. Govorkov, E. A. Kozhukhova, S. J. Pearton, F. Ren, L. Liu, J. W. Johnson, W. Lim, N. G. Kolin, S. S. Veryovkin and V. S. Ermakov, *J. Vac. Sci. Technol., B*, 2012, **30**, 061207.
27 A. Y. Polyakov, N. B. Smirnov, A. V. Govorkov, A. V. Markov, S. J. Pearton, N. G. Kolin, D. I. Merkurisov and V. M. Boiko, *J. Appl. Phys.*, 2005, **98**, 033529.
28 T. Egawa, H. Ishikawa, M. Umeno and T. Jimbo, *Appl. Phys. Lett.*, 2000, **76**, 3022.
29 S. J. Pearton, J. C. Zolper, R. J. Shul and F. Ren, *J. Appl. Phys.*, 1999, **86**, 1.
30 S. J. Pearton, Y.-S. Hwang and F. Ren, *JOM*, 2015, **67**, 1601.
31 B. D. Weaver, T. J. Anderson, A. D. Koehler, J. D. Greenlee, J. K. Hite, D. I. Shahin, F. J. Kub and K. D. Hobart, *ECS J. Solid State Sci. Technol.*, 2016, **5**, Q208.
32 J. L. Lyons and C. G. Van de Walle, *npj Comput. Mater.*, 2017, **3**, 12.
33 G. Kresse and J. Furthmüller, *Phys. Rev. B: Condens. Matter Mater. Phys.*, 1996, **54**, 11169.
34 J. Furthmüller and G. Kresse, *Comput. Mater. Sci.*, 1996, **6**, 16.
35 P. E. Blöchl, *Phys. Rev. B: Condens. Matter Mater. Phys.*, 1994, **50**, 17953.
36 J. P. Perdew, K. Burke and M. Ernzerhof, *Phys. Rev. Lett.*, 1996, **77**, 3865.
37 H. J. Monkhorst and J. D. Pack, *Phys. Rev. B: Solid State*, 1976, **13**, 5188.
38 G. Henkelman, B. P. Uberuaga and H. Jónsson, *J. Chem. Phys.*, 2000, **113**, 9901.
39 A. Kyrtsos, M. Matsubara and E. Bellotti, *Phys. Rev. B*, 2016, **93**, 245201.
40 A. Janotti and C. G. Van de Walle, *Phys. Rev. B: Condens. Matter Mater. Phys.*, 2007, **76**, 165202.
41 R. Wang, X. Tong, J. Xu, S. Zhang, P. Zheng, F.-X. Chen and W. Tan, *Phys. Rev. Appl.*, 2019, **11**, 054021.
42 S. A. Goodman, F. D. Auret, F. K. Koschnick, J. M. Spaeth, B. Beaumont and P. Gibart, *Mater. Sci. Eng., B*, 2000, **71**, 100.
43 H. J. von Bardeleben, J. L. Cantin, U. Gerstmann, A. Scholle, S. Greulich-Weber, E. Rauls, M. Landmann, W. G. Schmidt, A. Gentils, J. Botsoa and M. F. Barthe, *Phys. Rev. Lett.*, 2012, **109**, 206402.
44 A. Y. Polyakov, N. B. Smirnov, A. V. Govorkov, A. V. Markov, N. G. Kolin, D. I. Merkurisov, V. M. Boiko, K. D. Shcherbatchev, V. T. Bublik, M. I. Voronova, I.-H. Lee, C. R. Lee, S. J. Pearton, A. Dabirian and A. V. Osinsky, *J. Appl. Phys.*, 2006, **100**, 093715.

